DSS 14 Antenna Calibrations for GSSR/VLA Saturn Radar Experiments

C. N. Guiar
Ground Antennas and Facilities Engineering Section

R. L. Riggs
TDA Engineering

R. Stevens
Office of Telecommunications and Data Acquisition

M. Wert
TDA Mission Support and DSN Operations

DSS 14 pointing and gain were calibrated to support X-band bi-static radar observations of Saturn's rings. The observations used the Goldstone Solar System Radar and the National Radio Astronomy Observatory Very Large Array in Socorro, New Mexico.

The pointing calibrations were based on conscan offset data collected during Voyager 1 and 2 support passes. The conscan data show angle-of-arrival sensing with no bias and 0.3-mdeg 1-σ error. Using the calibrations, demonstrated blind pointing performance on Saturn was <3-mdeg 1-σ error.

Meteorological observations at the site were used to reduce elevation errors caused by atmospheric refraction. The techniques used corrected about one-third of the error—poorer than expected performance.

I. Introduction

This article describes the calibration of the beam pointing and the gain of the DSS 14 64-m antenna in preparation for a series of X-band (8.5-GHz) radar observations of the rings of Saturn. For the radar observations, DSS 14 illuminated the planet rings, and the VLA in Socorro, New Mexico, received the echo. The VLA used antennas that had been recently outfitted for X-band reception in preparation for support of the Voyager 2 Neptune encounter.

The plan for the work was developed in late March, 1987; the work was performed at DSS 14 during April and the first

three weeks of May. Radar observations of Saturn's rings were conducted May 23 through May 31.

The performance goals were ambitious: ≤2-mdeg 3-σ beam pointing error; ≤3-dB 3-σ absolute gain error.

A secondary objective of the work was to develop and demonstrate improved techniques for application to calibration of the DSN antennas for spacecraft mission support.

II. Summary

This report describes the calibration techniques used and presents the results obtained.

A. Techniques Used

The basic technique used for the pointing calibrations was to collect conscan data on a non-interference basis during Voyager 1 and 2 support passes. Also, beam scans were made of Saturn's thermal radiation. Then, the pointing calibrations obtained from the Voyager conscan tracks and the Saturn scans which used the "XRO" antenna feed cone were translated to the radar "XKR" feed cone.

To meet the elevation pointing accuracy objectives, an improved technique was required to correct for atmospheric refraction. The current technique is to calculate refraction bending based on average site meteorological conditions—referred to as default parameters. The approach used here was to make meteorological measurements at the site during a pass, and from them provide corrections to the values calculated for the default parameters.

Also, we aspired to develop some empirical data on wind induced pointing errors from the instrumented conscan tracks. On all tracks providing good conscan data the wind was, alas, benign; no useful data were obtained.

We used the measurement techniques developed by the 70-m Upgrade Project to determine the radar system receive configuration antenna efficiency.

B. Results Obtained

The pointing capability was demonstrated during the radar observations by short scans of the blackbody emission of Saturn using the radar receive mode feed. Saturn is a poor target for the purpose (approximately 6-mdeg disc diameter, approximately 1.1-K source temperature), but it was the best available technique for direct validation of the beam pointing.

Saturn scans were normally made twice in each radar pass during the period day-of-year (DOY) 145 through 164. That period included the Saturn rings and succeeding Titan moon observations. Averaging the results gave a worst beam pointing error of 5.9 mdeg and a mean error of 2.7 mdeg. The resulting 1-way degradation from pointing errors was 0.32 dB maximum, 0.09 dB mean. Clearly we did not meet the 2-mdeg 3-σ pointing error calibration goal. However, the degradation in quality of the radar observations resulting from DSS 14's pointing errors was evidently small.

In the time available, it was not possible to provide a sensitive receiving capability on the radar transmit mode feed, so its pointing could not be demonstrated, only inferred.

The effort to demonstrate better correction for atmospheric refraction was partially successful. Use of concurrent meteorological data reduced the average elevation errors during a pass by perhaps 30 percent—we expected much greater error reduction.

One set of antenna efficiency vs. elevation angle data was obtained for the radar receive mode. The results show a peak aperture efficiency of 46.7 percent at 42 degrees elevation. Lacking suitable coupling to the receiver, the measurement could not be accomplished for the radar transmit mode.

III. The DSS 14 Pointing System

A. Introduction

The techniques used for making and applying the antenna calibrations involve the operational pointing system and various off-line data collection and analysis tools. This section describes the basic pointing system. An end-to-end antenna pointing system block diagram is shown in Fig. 1; a glossary of abbreviations is given in Table 1.

B. Pointing by Predicts

The antenna is pointed based on target angle vs. time predictions prepared at the JPL NSS and transmitted to the Complex SPC prior to a tracking support pass. The predicts are computed from spacecraft or other celestial body ephemerides. They are in the form of topocentric direction cosines, and for spacecraft tracks they are supplied at ten minute intervals. In principle, the errors inherent in the predicts are completely negligible.

Before the tracking pass, the complex CMC Operator sends the antenna predicts to the APA. The APA transforms the direction cosines of the predicts to Az–El coordinates. The LMC Operator sends the Az–El predict points and an antenna pointing Systematic Error Correction Table (SETBL) from the APA computer disk to the antenna mounted ACS microcom-

puter. The ACS interpolates the predicts and provides angle position signals to which the antenna is slaved via either the MEC (for the Master Equatorial Precision mode) or the ASC (for the Computer Control backup mode). The Precision mode was used for all of our work.

Also, the antenna can be pointed from predicts aided by a scanning mode that senses, and corrects to, the true direction-of-arrival of the radio signal. That mode is conscan (for conical scanning); it can sense and correct errors as large as the half-power beamwidth of the antenna.

C. Pointing by Conscan Aided Predicts

Conscan works in the following way. The APA generates a circular scan pattern for the antenna and sends it to the ACS. The ACS adds the scan pattern to the corrected pointing predicts. Software in the REC computes and sends received signal levels to the APA via the SPC LAN.

The correlation of the scan position of the antenna, as reported by the ACS, with the received signal level variations allows the APA to compute corrections to the scan pattern center. The APA sends the corrections to the ACS. Thus, within the capability of the closed-loop control system, the scan center is pointed precisely to the apparent direction-of-arrival of the spacecraft signal.

As will be discussed in the following section, the offsets between the signal direction-of-arrival as computed by conscan, and the direction defined by the corrected pointing predicts, provided the source for most of our calibration data.

IV. Conscan Offset Data Collection, Reduction, and Analysis

A. Introduction

During the period for making the pointing calibrations, DSS 14 was heavily loaded with spacecraft mission support. It was necessary that our data collection be a non-interfering by-product of that support. Conscan is the normal operational antenna mode for spacecraft support at X-band. We used non-intrusive data capture programs to collect conscan offset data from the channel between the APA and the ACS.

The basic approach in using the spacecraft conscan offset data is to presume that the predicts are correct and that conscan correctly senses the direction of the signal. Then, any systematic offsets are attributed to systematic pointing errors of the antenna beam.

Because conscan offsets were the basic source of calibration data, we did some analyses to characterize their quality. That work is presented in Appendix A.

B. Conscan Data Collection and Processing

1. **Background.** Voyager 2 and Saturn are nearby in the sky—separated by about an hour in right ascension and 2 deg in declination. Therefore, Voyager 2 data were directly applicable to the Saturn pointing calibrations; Voyager 1, which reaches 65 deg elevation at DSS 14, provided data to stabilize the calculation of the antenna systematic error parameters.

During the period DOY 086 to 142, conscan offset data were collected on 21 Voyager passes—all but a few of the scheduled support passes. Those few passes were designated by the Voyager Project as involving critical support.

Preliminary conscan data were obtained from DOY 086 to 099; various problems with the pointing system were experienced from DOY 104 to 118, and the data obtained during that period were of little use. From DOY 120 to 139 good data were obtained from two Voyager 1 and three Voyager 2 passes, and from one pass observing Saturn's thermal radiation. Those data were the basis for the antenna Systematic Error Table (SETBL) developed for the Saturn radar observations.

Figure 2 shows the mean offsets of the raw conscan data from the Voyager tracks during the period DOY 086 to 142. The period of faulty pointing system performance is evident.

2. **Techniques used.** Figure 3 illustrates the sequence of steps used to collect the conscan data and to develop the antenna pointing error model and SETBL. The steps are described in the following paragraphs. The software programs involved are developmental, not in the operational DSN library.

The CAPTURE program accesses the antenna information transmitted between the APA and the ACS via a monitor port on the APA modem patch panel. Time tagged azimuth and elevation angles and azimuth and elevation conscan offsets are logged to a file and displayed on the monitor and line printer. The data collection is not in-line; it is accomplished without interference during mission support tracking.

The PLOTSCAN and CONPLOT programs provide plots of the conscan offset data. PLOTSCAN plots cross-elevation, elevation, and beam pointing offsets versus azimuth angle. CONPLOT plots azimuth, elevation, and cross-elevation offsets versus time.

The plots allow immediate assessment of the conscan offset data quality. Bad or suspicious data can be easily identified for file editing prior to using the record for calibration purposes.

Statistical analysis of the conscan data file is provided by ANA-CON. The mean and standard deviation (σ) of the azimuth, elevation, cross-elevation, and beam pointing offsets are calculated. Also, signal losses in decibels from the beam offsets are determined, and offsets exceeding 3σ are identified.

The edited conscan data file is input to READCON. READCON outputs an offset file in a format suitable to input to CONCORR for computing refraction correction, and to input to PHO9 for computing the parameters of the antenna pointing systematic error model. The techniques used for computing refraction correction, and the results obtained, are discussed in detail in Appendix B.

The PHO9 program works best with 50 to 100 input points. A typical conscan offset raw data file from an 8-hour Voyager track has about 300 points. Also, data from tracks on several days normally are used to compute a set of model parameters. To reduce the size of a conscan offset data input file for PHO9:

(1) All data from periods when conscan is not functioning stably are edited out, as previously discussed;

(2) Selected sections of tracks from different days are used;

(3) To further reduce the file size, every other sample of a record is deleted. That process provides less smoothing of the conscan offset data (estimated 1σ of 0.3 mdeg with all data points vs. 0.5 mdeg with deletions)—it was used for simplicity in preparing the file.

V. Techniques for Development of Systematic Error Correction Tables

A. Introduction

The pointing error modeling approach used in the DSN is based on expected physical behavior of the antenna. It was developed by optical and radio astronomers; it has been successfully applied to major radio astronomy facilities [1].

The complete pointing error model for an antenna is a sum of separate error functions. Table 2 shows the individual error sources and the elevation and cross-elevation error functions used to develop the complete model systematic error correction table. The functions in Table 2 apply for the "precision" mode which uses the Master Equatorial as the pointing reference.

B. Techniques Used

The observational data are used by the PHO9 error model program to generate or refine an antenna systematic pointing error model. PHO9 determines the "P" constants in the individual error functions of Table 2.

PHO9 reads the edited conscan offset data file. It then sums the offsets from the a priori error model—the systematic error correction model used during the track—with the conscan offsets, resulting in the total offsets due to systematic errors. Finally, PHO9 uses a linear least squares fitting routine to compute the "P" parameters of the new systematic error model.

Programs are available that provide display of the systematic error model and its parameters. PLOT'MDL plots the systematic error model versus hour angle for a specified declination. PRMDLANL prints the model "P" parameters and the quality of their determination by the PHO9 fitting. TABLES tabulates azimuth and elevation offsets of a systematic error model at 5-degree increments of azimuth vs. elevation.

Finally, the SECPHO program takes a set of model parameters and calculates a Systematic Error Correction Table (SETBL). The output of SECPHO is a suitably formatted file that is loaded into the ACS via the APA using a VT-100 simulator program. The last step provides the SETBL for operational use.

VI. Final Development of Systematic Error Correction Table for Use in GSSR/VLA Saturn Radar Experiment

A. Introduction

Conscan offset data from five Voyager passes late in the period (DOY 120, 125, 126, 127, and 136) appeared good. They were the basis of our final SETBL. The statistics of the error data for these days are given in Table 3.

B. Process of SETBL Development

A SETBL was developed using the data from the passes on DOY 120, 125, 126, and 127. The SETBL table used during each of those tracks was M4X31N; its "P" parameters are given in Table 4. The data from each of the four cited days were edited by the methods described in the previous section and merged into one file. The SETBL calculated from that file was M4X31B; its "P" parameters are also given in Table 4.

SETBL M4X31B was used during the track on DOY 136 with results as shown in Table 3. Then, the data from DOY 136 were edited and merged with the data file used to generate SETBL M4X31B, and that revised file was used to generate the set of "P" parameters M4X31C (cf. Table 4).

On DOY 139, the blackbody (thermal radiation) from Saturn was scanned using SETBL M4X31C. The results are shown in Fig. 4—the mean cross-elevation offset is -1.1 mdeg; the mean elevation offset is +4.0 mdeg.

We reviewed the recent results from Voyager passes and the Saturn track and decided to accept the -1.1 and +4.0 mdeg mean offsets. These offsets were added to the P1 and P7 terms, respectively, to form the "P" parameter set M4X31C(REV) (cf. Table 4). M4X31C(REV) was our final version of the systematic error correction for the antenna using the "XRO" Cassegrain cone.

The SETBLs were based on Voyager conscan and Saturn offset data using the "XRO" Cassegrain cone. However, the "XKR" Cassegrain cone is used for radar measurements. The antenna beam using the "XRO" cone is slightly offset from the beam using the "XKR" cone—the offset must be accounted for in applying the pointing calibrations to the radar. The correction is made by adjusting the beam collimation error parameters:

$$P1(XKR) = P1(XRO) + 0.0105 \text{ (deg)}$$

$$P7(XKR) = P7(XRO) + 0.0045 \text{ (deg)}$$

The above corrections are based on previous measurements at DSS 14 by D. Girdner.

VII. Beam Pointing Measurements During Period of Radar Observations

Beam pointing was checked regularly during the period of the radar observations using beam scans of Saturn's blackbody radiation. Usually we made one check at the beginning and one check at the end of each radar track. With the aid of a simple program on a PC, it took about 10–15 minutes to complete a set of scans and estimate the beam error indicated by the data.

These measurements used the Noise Adding Radiometer (NAR) and the Square Law Detector Assembly (SQLD) in the GSSR equipment room in the pedestal. The microwave system and the receiver front end were as configured for the radar track.

The results from the beam pointing checks from Saturn scans are shown in Figs. 5 (antenna temperature from Saturn's radiation), 6 (cross-elevation error), and 7 (elevation error). The data shown were taken during the period of the radar observations of Saturn's rings, and during a subsequent period of radar observations of Saturn's moon, Titan.

From the average cross-elevation and elevation errors of the preceding figures, we calculate the average beam errors (Fig. 8), and from those, estimate the one-way loss from pointing errors. The loss results are shown in Fig. 9. The worst loss on a day is 0.32 dB; the mean and median losses for the 12 days are 0.09 dB and 0.05 dB, respectively. We expect those results are representative of the pointing performance during the actual radar observations.

VIII. Antenna Efficiency Measurements of the Radar (XKR) Feed Cone

Our original intention was to calibrate the antenna with both the transmit and receive radar feeds. We were unable to provide a satisfactory receiving configuration for the transmit feed, and therefore did not accomplish its calibrations.

Antenna efficiency measurements were taken of the radar receive feed at the radar operating frequency, 8,495 MHz. The measurements were made on DOY 134. The experimental procedures used were those recently developed for the efficiency measurements of the large antennas before and after their upgrade from 64 m to 70 m.[1] Figure 10 is a functional block diagram of the equipment used.

The results of the efficiency measurements are shown in Fig. 11. The curve is a mean square quadratic fit to the circled data points. The maximum efficiency was 46.7 percent at 42 degrees elevation.

IX. Conclusions

(1) Conscan offset data were collected and analyzed on a noninterference basis during Voyager support passes. Using that data and a few hours of noisy Saturn beam scan data, blind pointing of 2 to 3 mdeg mean beam error was provided. That beam error results in <0.1 dB mean one-way degradation for the radar.

[1] K. Bartos, et al., "Antenna Gain Calibration Procedure," JPL D-3794 (internal publication), Jet Propulsion Laboratory, Pasadena, California, November 15, 1986.

(2) When the system is functioning normally, conscan points the antenna in the direction of the received signal with essentially no bias and about 0.3 mdeg standard deviation (see Appendix A). That is very high quality pointing calibration data.

The operational conscan system needs an improved protocol for setting and demonstrating its closed loop parameters.

(3) The improvement in elevation pointing accuracy from use of concurrent surface atmospheric measurements for the refraction correction was less than expected (see Appendix B). The results we obtained were really not suitable for the precision pointing and calibration of 70-m apertures at X and Ka bands.

The techniques involved must be improved in the future.

(4) A configuration to allow direct measurement of the pointing and gain of the radar transmitter feed must be provided.

Reference

[1] R. Stevens, R. L. Riggs, and B. Wood, "Pointing Calibration of the MKIVA DSN Antennas for Voyager 2 Uranus Encounter Operations Support," *TDA Progress Report 42-87*, vol. July–September 1986, Jet Propulsion Laboratory, Pasadena, California, pp. 206–239, November 15, 1986.

Table 1. Glossary of abbreviations for text and figures

ACM	Antenna control and monitor
ACS	Antenna control subassembly
APA	Antenna pointing assembly
ARA	Area routing assembly
ASC	Antenna servo controller
CMC	Central monitor and control (console)
FEA	Front end area
IRS	Intermediate reference structure
LAN	Local area network
LMC	Link monitor and control (console)
MDA	Metric data assembly
MEA	Master equatorial assembly
MEC	Master equatorial controller
MMA	Meteorological monitoring assembly
NAR	Noise adding radiometer
NASCOM	NASA communications
ND	Noise diode
NSS	Network support subsystem
PC	Personal computer (IBM compatible)
REC	Receiver-exciter controller
SETBL	Systematic error table
SPC	Signal processing center
TWM	Traveling-wave maser

Table 2. Systematic pointing error model for 64-m antenna (precision mode)

Error	Cross-elevation model	Elevation model	Cross-declination model	Declination model
Cross-elevation collimation	P1	–	–	–
Elevation collimation	–	P7	–	–
Gravity flexure	–	P8cos (el.)	–	–
Hour angle declination orthogonality	–	–	–P11sin (dec.)	–
Hour angle axis alignment	–	–	P12sin (h angle) sin (dec.)	P12cos (h angle)
Hour angle axis alignment	–	–	–P13cos (h angle) sin (dec.)	P13sin (h angle)
Declination encoder bias	–	–	–	P16
Hour angle encoder bias	–	–	P21cos (dec.)	–

Table 3. Conscan error statistics for DOYs 120, 125, 126, 127, and 136

DOY	SETBL	Cross-elevation		Elevation		Number of points
		Average	σ	Average	σ	
120	4X31N	-0.3	1.1	1.1	1.9	102
125	4X31N	-1.4	1.1	-2.5	0.8	33
126	4X31N	2.5	0.7	0.5	0.8	27
127	4X31N	-2.1	0.7	1.3	1.1	45
136	4X31B	-2.6	0.7	0.6	1.1	16

Table 4. Systematic error correction table parameters (degrees)

Parameter number	M4X31N	M4X31B	M4X31C	M4X31C (REV)
1	-0.00389	-0.00031	-0.00349	-0.00459
7	0.02018	0.02756	0.02555	0.02955
8	-0.03179	-0.03806	-0.03782	-0.03782
11	0.00647	0.00000	0.00000	0.00000
12	0.00000	-0.00213	0.00079	0.00079
13	0.00000	-0.00357	-0.00067	-0.00067
16	0.00126	0.00121	0.00064	0.00064
21	-0.00664	-0.00743	-0.00564	-0.00564

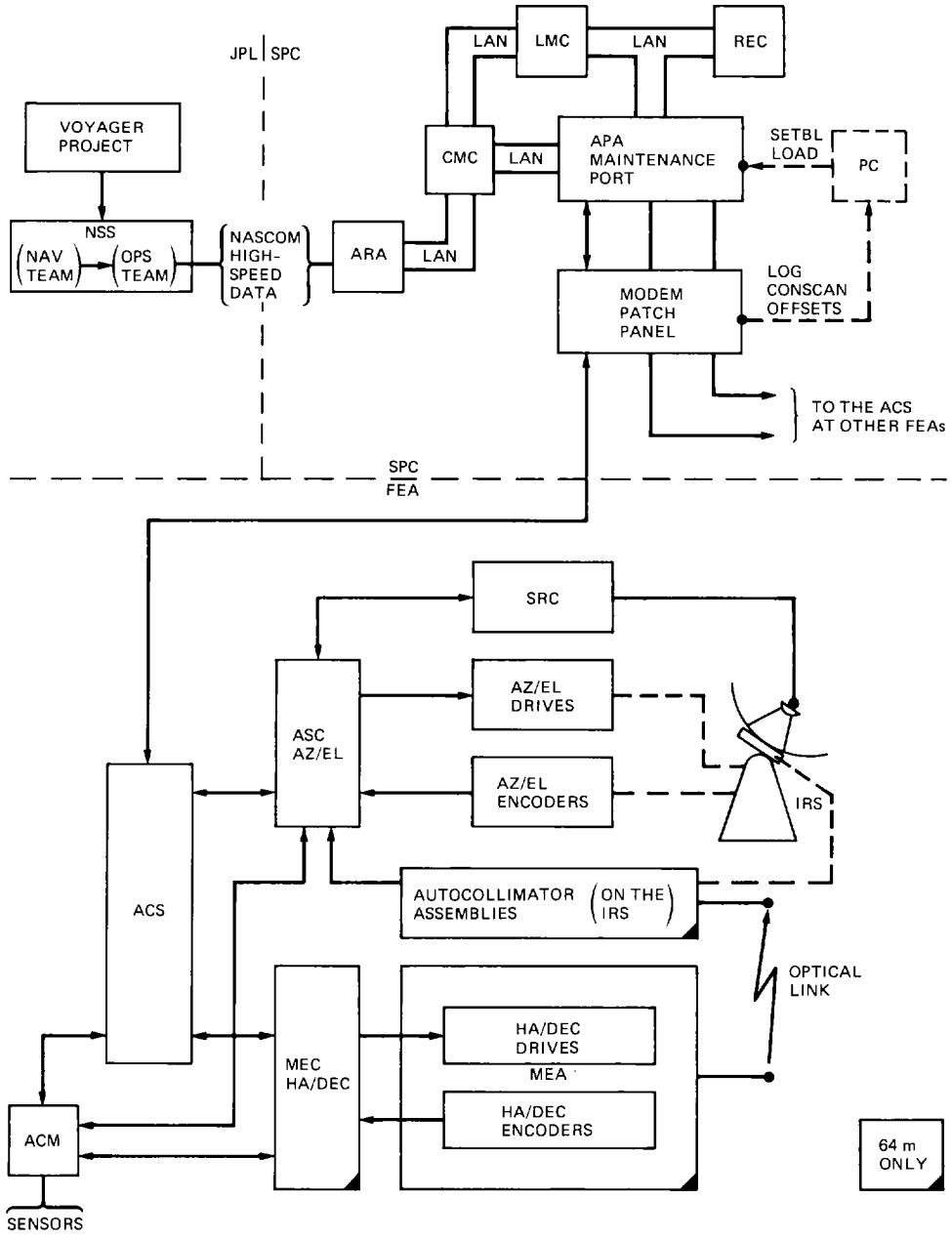

Fig. 1. DSS 14 end-to-end antenna pointing system

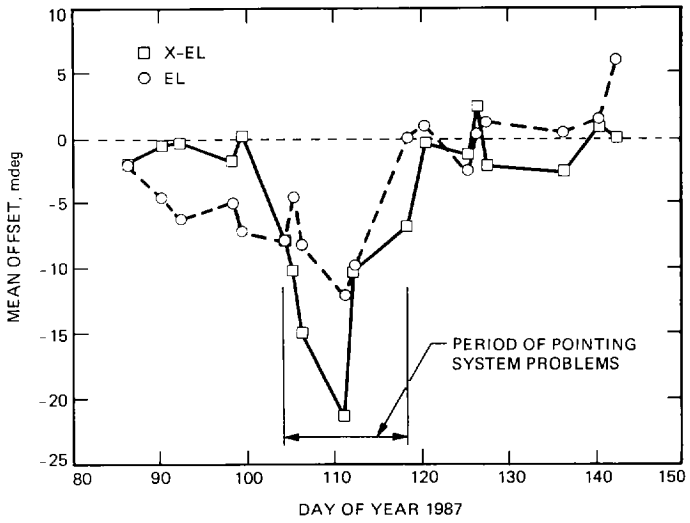

Fig. 2. Conscan offsets from Voyager tracks

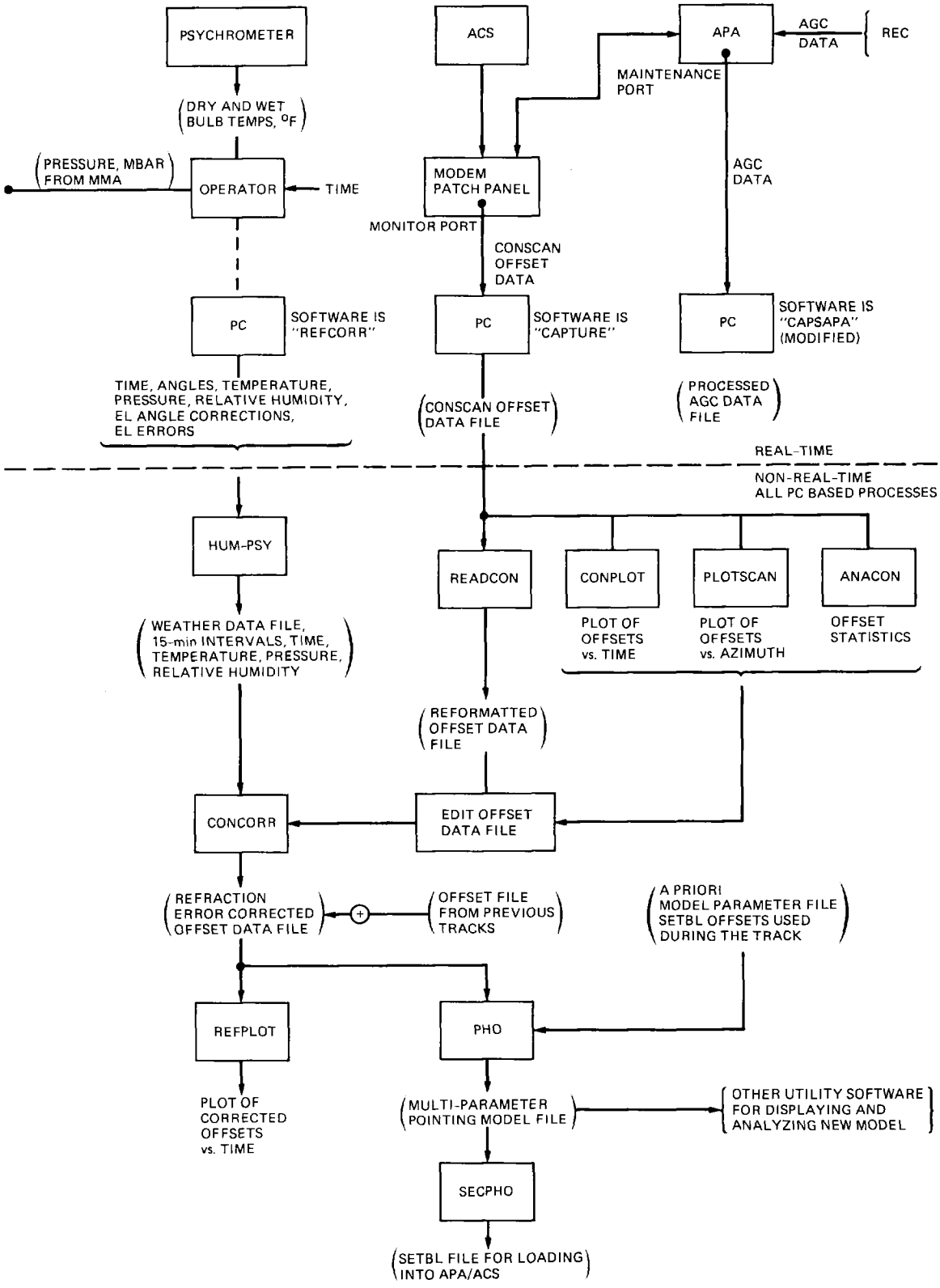

Fig. 3. Block diagram of conscan data acquisition and data processing

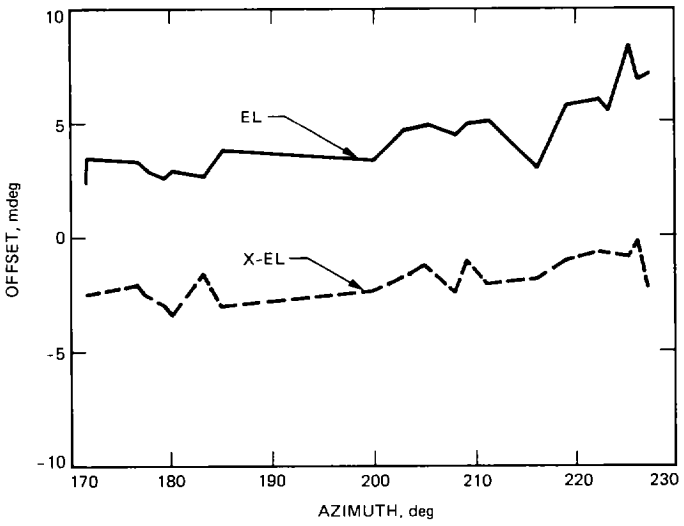

Fig. 4. Cross-elevation and elevation from Saturn blackbody scans on DOY 139

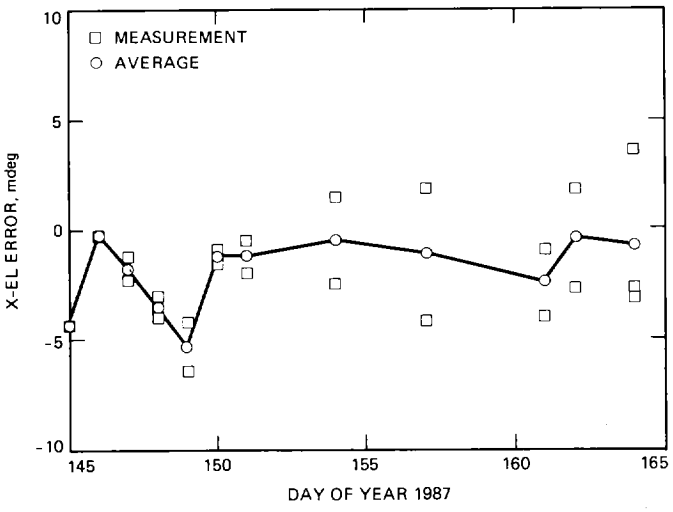

Fig. 6. Cross-elevation errors from Saturn scans

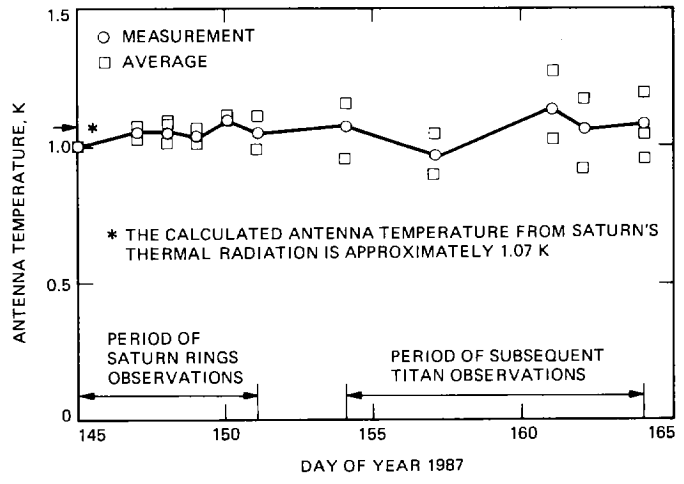

Fig. 5. Antenna temperature from Saturn blackbody radiation observations

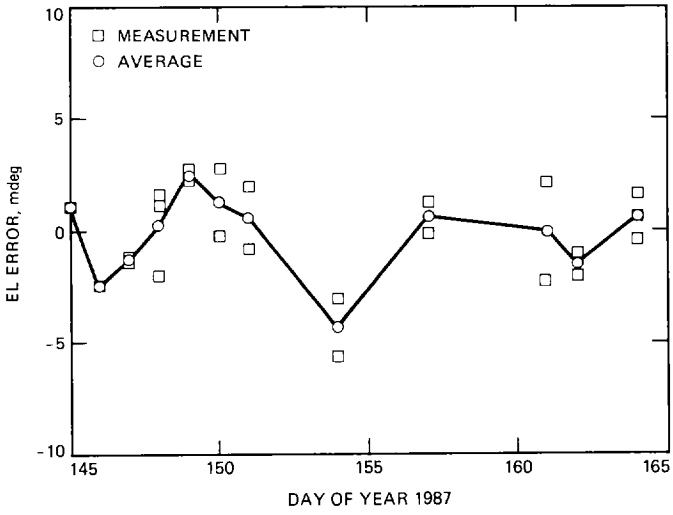

Fig. 7. Elevation errors from Saturn scans

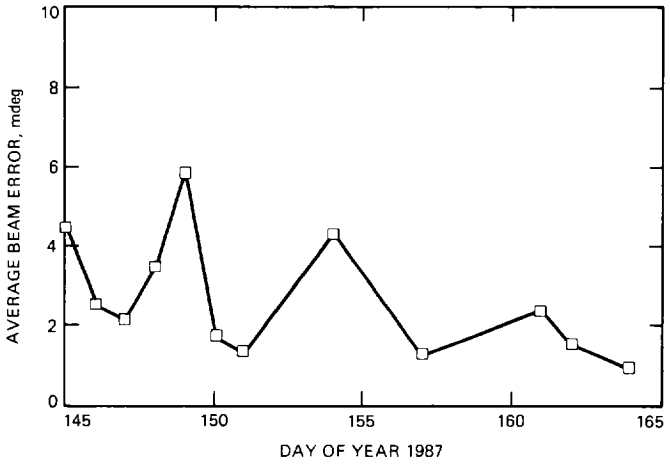

Fig. 8. Average beam pointing errors from Saturn scans

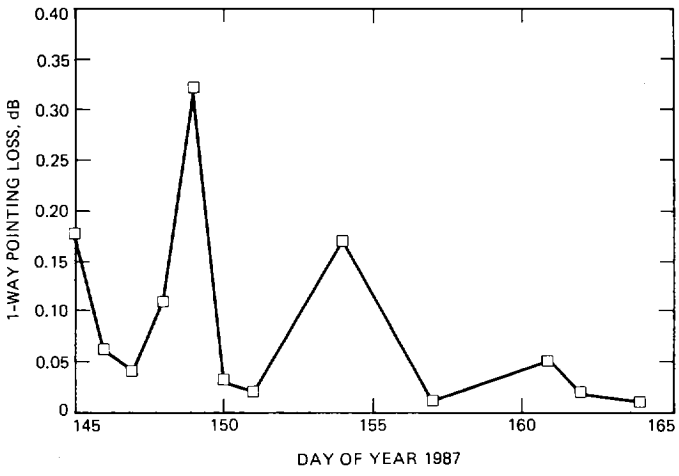

Fig. 9. Average pointing loss calculated from Saturn scans

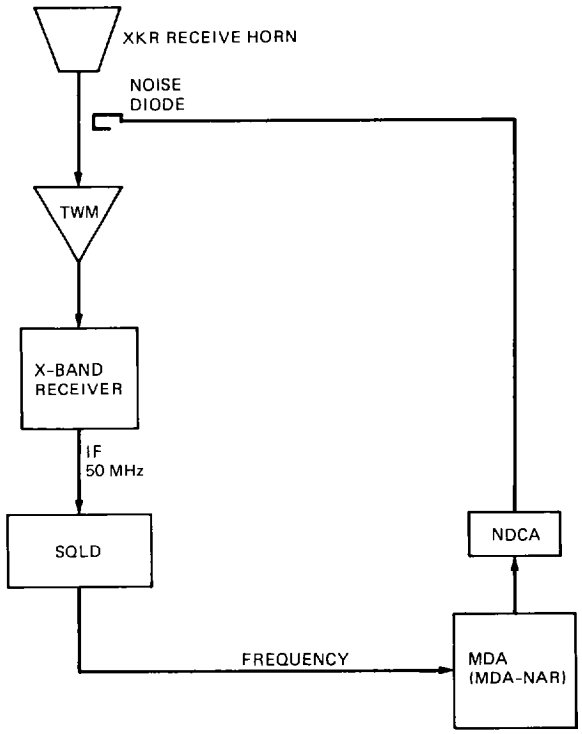

TWM = TRAVELLING WAVE MASER
SQLD = SQUARE LAW DETECTOR
MDA = METRIC DATA ASSEMBLY
NDCA = NOISE DIODE CONTROL ASSEMBLY
IF = INTERMEDIATE FREQUENCY

Fig. 10. Functional block diagram of antenna efficiency measurement equipment

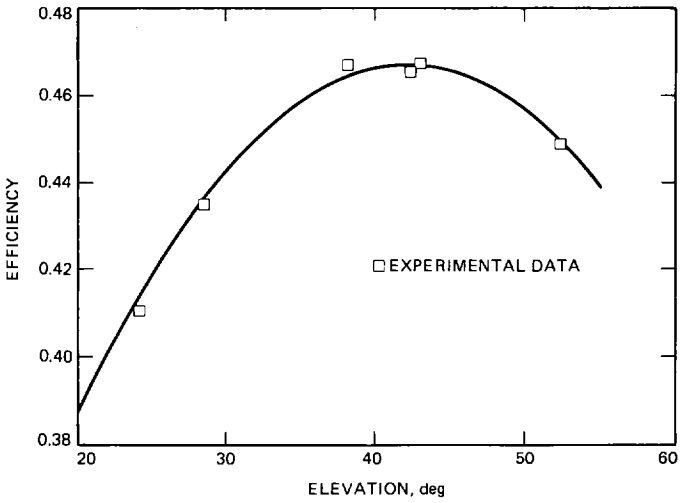

Fig. 11. Antenna efficiency of XKR cone receive feed

Appendix A

Experimental Investigation of Conscan Performance

I. Introduction

Conscan offset data from spacecraft tracking were used to determine the systematic errors in antenna pointing. We have done analyses to assess some of the quality parameters of the data.

Conscan performance is affected by signal level variations that are not due to ground antenna pointing (e.g., changes in ground system gain, changes in spacecraft antenna pointing and radiated carrier power). To characterize those effects empirically, we examined the conscan performance during a high activity Voyager pass that included changes in the telemetry modulation index and changes in spacecraft attitude limit cycle amplitude.

Also, we examined the detailed signal level variations and related angular offsets during conscan acquisition and tracking. We obtained estimates of response and smoothing time, pointing jitter, and pointing bias for the conscan system.

The instrumentation and data analysis techniques used and the results obtained are reviewed in this Appendix. However, before proceeding, we review some basics of the conscan system.

II. A Primer on Conscan Technical Performance

The source document for this discussion is [A-1].

When the conscan axis is offset from the exact direction of arrival of the signal, amplitude modulation of the receiver output at the scan frequency results. For small offsets, the offset between the conscan axis and the direction of signal arrival is a constant multiplier of the modulation amplitude in decibels. The constant is determined by the scan radius and the antenna half-power beamwidth (3.0 mdeg and 36 mdeg, respectively, at DSS 14); it is approximately 9.0 mdeg/dB (peak-to-peak).

In the MKIVA implementation of conscan[1] the magnitude and orientation of the angular offset are calculated by cross-correlation of the signal modulation with the scanning waveform. The calculation is made for each scan cycle by a Fast Fourier Transform. The calculation must have an appropriate scale factor, "A," to faithfully convert the modulation in decibels to equivalent angular offset in millidegrees—"A" embodies the antenna beam's mdeg/dB noted above, and the gain and scan period integration time of the correlation calculation. "A" can be determined experimentally by observing the correlator output while conscanning on a target with a fixed and known offset.

We define [A × offset (1)] as the correlator output from the scan with the conscan axis having offset (1). The conscan system forms the subsequent offsets to be sent to the antenna as:

$$\text{offset}(2) = \text{offset}(1) - h \times A \times \text{offset}(1)$$

or

$$\text{offset}(2) = \text{offset}(1) \times (1 - h \times A)$$

and so forth.

The parameter "h" is a gain selected such that $0 < (1 - h \times A) < 1$.

Rewrite the above relation as:

$$\text{offset}(2) / \text{offset}(1) = (1 - h \times A)$$

which illustrates that conscan reduces each subsequent offset by the factor $(1 - h \times A)$; the nth offset is given by:

$$\text{offset}(n) / \text{offset}(1) = (1 - h \times A) \wedge (n - 1) \qquad \text{(A-1)}$$

A useful measure of the closed loop dynamic response of conscan is the time, τ, to reduce an initial offset by 1/e. If N is the number of P second scans—following the initial scan—required for the reduction, then:

$$\text{offset}(N + 1) / \text{offset}(1) = 1/e = (1 - h \times A) \wedge (N)$$

$$N = -1 / \log (1 - h \times A)$$

and

$$\tau = N \times P \qquad \text{(A-2)}$$

in seconds.

[1] J. R. Smith, "Conscan," unpublished notes, Jet Propulsion Laboratory, Pasadena, California, October 23, 1984.

For example, a $(1 - h \times A)$ of 0.95 gives N = 19.5 scans, which for a 32-second scan period gives τ = 624 seconds, or 10.4 minutes. An initial offset is reduced by factors 0.36 (1/e) after one τ, 0.14 after two τ, 0.05 after three τ; for practical purposes, an acquisition or reacquisition is complete after two to three τ seconds.

The effects on conscan data quality from noise on the signal level are a complicated matter. Some aspects of the matter are treated in detail in [A-1]; for present purposes we take one basic result: the random angular jitter from a single scan is reduced by the square root of N for continuous closed loop conscan tracking.

III. Conscan Performance During a High Activity Voyager Pass

The CAPSAPA program, developed by D. Kiewicz, logs time tagged carrier signal level data from the APA maintenance port on a noninterference basis during a pass. We used CAPSAPA to collect and display signal level data from several Voyager passes.

Figure A-1 shows smoothed signal level vs. time for the DOY 086 Voyager 2 pass. There were several spacecraft mode change events during the pass. The spacecraft events, including attitude limit cycle changes, link 1-way/2-way changes, and modulation index changes, are annotated in the figure.

Figure A-2 shows conscan offsets recorded during the DOY 086 pass. The spacecraft events and the conscan on/off periods are annotated in this figure, also.

Examination of Figs. A-1 and A-2 shows:

(1) The spacecraft attitude limit cycling does not significantly affect the conscan performance (refer especially to the period 1030 to 1140 GMT)—that is as expected, considering that the spacecraft period is 15 to 30 minutes, whereas the conscan period is 32 seconds;

(2) A significant change in signal level that occurs within a conscan period will result in a significant transient in the conscan offsets (refer to the spacecraft mod index change at 1630 GMT);

(3) When conscan is turned off prior to a significant spacecraft event, and the conscan offsets are retained, pointing will continue quite smoothly when conscan is turned back on (refer to the mod index change event at 1220 GMT, and the receiver O/L event at 1555 GMT; compare that with the receiver O/L event at 1155 GMT when the conscan offsets were zeroed out before turning conscan back on);

(4) Conscan system acquisition or settling time during the pass is 15–20 minutes (refer to the initial acquisition at 1020 GMT, and the transients at 1155 and 1630 GMT in Fig. A-2). Also, the peak-to-peak deviation about a smoothed version of the offsets in both axes is indicated as approximately 1 mdeg (see Fig. A-2). This performance is generally representative of that observed on the Voyager passes that did not have known system problems.

During the initial phase of conscan data collection we analyzed several Voyager passes in the way discussed above. We soon concluded that it was not necessary to collect signal level data in order to do reliable editing of the conscan offset files for use in determining systematic pointing errors. The required editing—elimination of conscan transient periods, and of conscan off or malfunctioning periods—could be done by examination of the conscan offset raw data plots, plus station logs and spacecraft event schedules.

However, we continued collection of signal level data; the data were used to help characterize conscan system performance. That work is presented in the next section.

IV. Performance of Conscan in Normal Acquisition and Tracking

A. Analysis of Conscan Acquisitions

Figure A-3 shows the scan modulated receiver output during the first conscan acquisition of Voyager 2 on DOY 086. The data are 5-second samples of the received signal level as logged by CAPSAPA. Spectral analysis of the noisy data shows that the regular variation is the 32-second conscan period.

The amplitude of the scan modulation decays as the acquisition proceeds. The estimated envelope of the modulation is sketched in the figure—it is about 0.28 dB at the start and about 0.16 dB after twelve scans. From that sample we estimate $(1 - h \times A) = 0.95$, and τ = 10.4 minutes using Eqs. (A-1) and (A-2) from Section II. Examination of the recorded conscan angular offsets for the same period shows consistent behavior: about 2.4 mdeg decaying to 1.6 mdeg, which when converted by the 9 mdeg/dB agrees with the modulation dBs.

Figure A-4 shows a similar signal level plot during a conscan reacquisition of Voyager 1 on DOY 118. From these data we estimate $(1 - h \times A) = 0.88$, and τ = 4.3 minutes. Again the recorded conscan offsets were found to be consistent with the behavior of the signal level modulation.

The closed loop response is quite different for the two tracks discussed above—no doubt a result of different con-

scan parameter settings. Unfortunately, we did not keep careful records of the parameters in use, nor did we perform pre-pass tests to experimentally determine the constants "h" and "A." Therefore, we cannot say whether or not the conscan dynamic performance was as it should have been.

In a later section (V.B), we outline proper calibrations of the conscan system to qualify its performance. In hindsight, we should have performed such calibrations at intervals during the conscan offset data collection work.

B. Analysis of Conscan Tracking

The CAPSAPA program can be used to make an estimate of the amplitude of the scan period sine wave found in a scan period length of the signal level record. CAPSAPA can then calculate the beam error (BE) corresponding to the sine wave amplitude (using the 9 mdeg/dB) and display and store the estimates for each scan cycle. The total beam error angular offset as derived from each scan period is resolved into two orthogonal components, BE1 and BE2, relative to the signal level record. (The CAPSAPA estimation is analogous to the cross-correlation calculation performed each scan cycle by the conscan system. It provides an independent assessment of the functioning of the conscan system.)

Figure A-5 is a plot of angular errors calculated by CAPSAPA as described above for 1,983 individual scan cycles. The data are from Voyager 1 and 2 passes of DOYs 118, 125, 127, 132, and 136.

Some statistics of the data in Fig. A-5 are:

	BE1	BE2
Mean	−0.00 mdeg	−0.02 mdeg
σ	1.13 mdeg	1.27 mdeg

The most significant characteristic of the data is that the means are essentially zero, as they should be if conscan is operating properly without biases. The cause of the non-circular pattern of the data in Fig. A-5 is not yet understood.

The total beam error should be approximately Rayleigh distributed. The probability function of BE for the data of Fig. A-5 is shown in Fig. A-6; it has a standard deviation of 1.7 mdeg. For example, to show the similarity, a Rayleigh distribution function, fit by inspection to the BE data, is also plotted; it has a standard deviation of 1.4 mdeg.

The cumulative probability functions for the BE data and the example Rayleigh distribution are shown in Fig. A-7.

Recall from the earlier discussion in Section II that the jitter on a single scan is reduced by the square root of N, the number of scans during the period of one closed loop time constant, τ. Thus, to relate the statistics of the single scan errors developed above to the actual conscan offset jitter observed, we must estimate N. From the records of ten passes we found an average value for τ of about 11 minutes. For a scan period of 32 seconds, the average N is 20, giving root N of 4.5. Thus, assuming Rayleigh distribution properties, we should see a standard deviation on BE of the conscan offset data of 1.7/4.5 = 0.4 mdeg.

Inspection of the complete conscan offset data records from two typical passes, one quiet, one noisy, showed peak-to-peak jitter in each axis of about 1.0 mdeg. There are about 100 independent samples in each conscan error record, so we estimate error standard deviation as the (peak-to-peak)/5. That gives 0.2 mdeg per axis, or a Rayleigh distributed BE with 0.3 mdeg standard deviation.

The angle jitter as calculated from the signal level modulation (0.4 mdeg) and that observed from the actual conscan offsets (0.3 mdeg) agree reasonably.

V. Observations on Conscan Performance

A. Quality of Offset Data for Antenna Pointing Calibrations

From the discussion presented, we conclude the following:

(1) All periods of transient or anomalous conscan performance can be identified and must be deleted from an offset file before it is used as pointing calibration data.

(2) A properly prepared conscan offset file provides true angle of arrival of the signal to about 0.3 mdeg BE standard deviation. The biases appear to be completely negligible.

B. Calibrations of the Conscan System

There are some straightforward calibrations that should be performed on the conscan system to ensure that its performance is proper and understood. The frequency of performing the calibrations needs to be determined by experience with the stability of the system—certainly they should be a part of preparing for antenna pointing calibration work, and for operations requiring guaranteed high performance of the conscan system.

We only describe the concept of the calibrations. The actual procedures for their accomplishment need to be worked out by DSN system engineering and operating personnel.

(1) *Open loop determination of system gain constants.* With the conscan loop open, set in a known offset (e.g.,

10 mdeg for the 64-m at X-band) in one axis and measure the value of the constant "A"; repeat in the other axis. Similarly, determine the product h × A; "h" should be set to provide a desired closed loop time constant as determined by (1 – h × A).

(2) *Open loop determination of axis cross-coupling.* Perform as in (1) but observe the offset signal in the orthogonal axis. Repeat with the other axis. The conscan phase delay should be adjusted so that the angular cross-coupling is <5 percent.

(3) *Observation of closed loop behavior–"snap-on-tests."* Set in a 10 mdeg offset in one axis and then close the conscan loop. Observe the decay of the offset. It should have a time constant within 10 percent of that expected from the value of (1 – h × A). Repeat with offsets in the opposite direction, and for the other axis.

During the snap-ons, observe the activity of the orthogonal axis. It is expected to display some cross-cross coupling even though the static setting is correct.

(4) *Validation that the conscan axis and the beam maximum coincide.* Establish stable conscan tracking on a spacecraft providing a steady signal level. Turn off conscan (leave offsets in), and perform beam scans ±10 mdeg in each axis.

C. Other Investigations Identified

(1) To understand and demonstrate the dynamic behavior of the MKIVA conscan system, an appropriate computer simulation model should be developed. The model would be run for the envelope of values of the (1 – h × A), scan period and width, and receiver time constant parameters, in the presence of noise.

(2) To develop the optimum conscan closed loop time constant settings for various support needs, e.g., rapid acquisition, or very low jitter tracking, a series of snap-on tests with various settings of the operating parameters should be performed and analyzed at the stations.

The simulation results would be used to guide the development of the tests at the stations, and to verify or interpret the test results.

References

[A-1] J. E. Ohlson and M. S. Reid, *Conical-Scan Tracking With the 64-m-diameter Antenna at Goldstone*, Technical Report 32-1605, Jet Propulsion Laboratory, Pasadena, California, October 1, 1976.

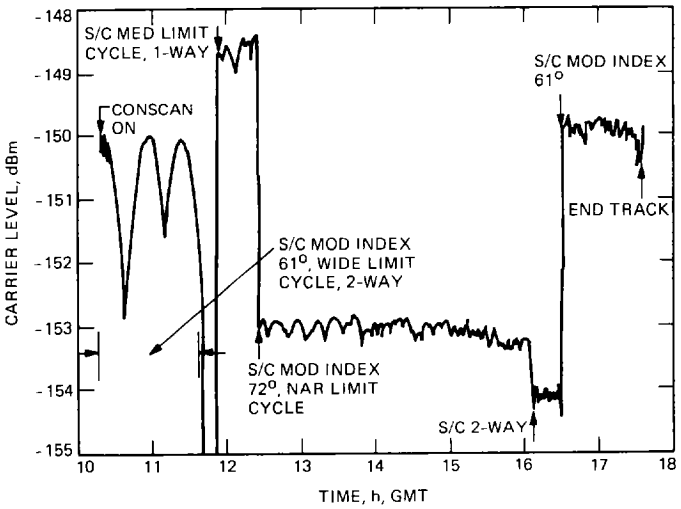

Fig. A-1. Carrier signal level: Voyager 2, DOY 086

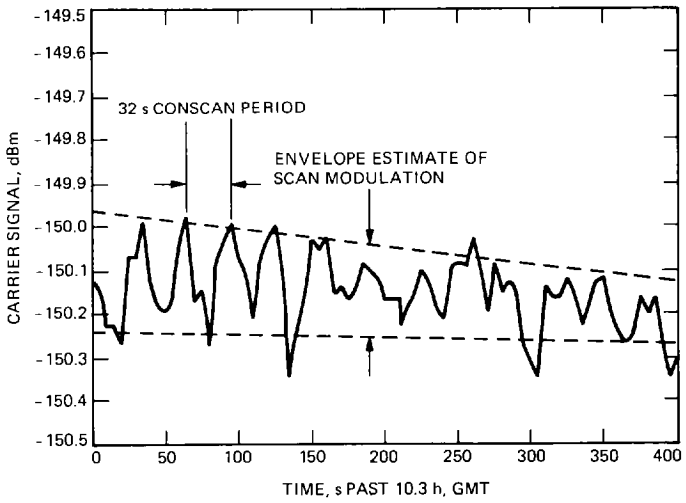

Fig. A-3. Carrier signal level vs. time during conscan acquisition: Voyager 2, DOY 086

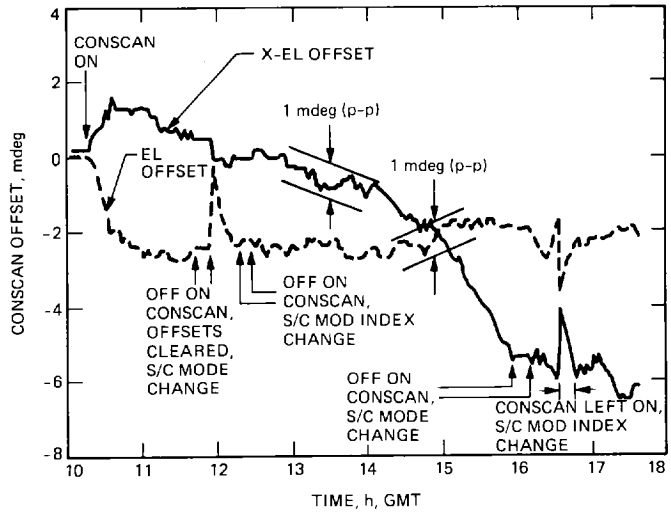

Fig. A-2. Conscan offsets: Voyager 2, DOY 086

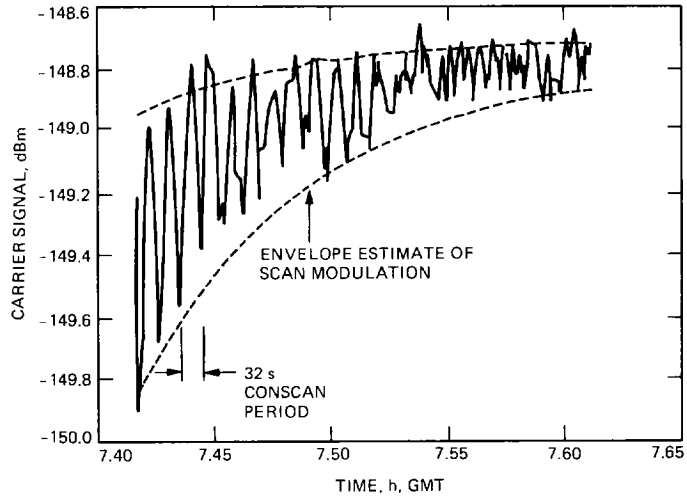

Fig. A-4. Carrier signal level vs. time during conscan acquisition: Voyager 1, DOY 118

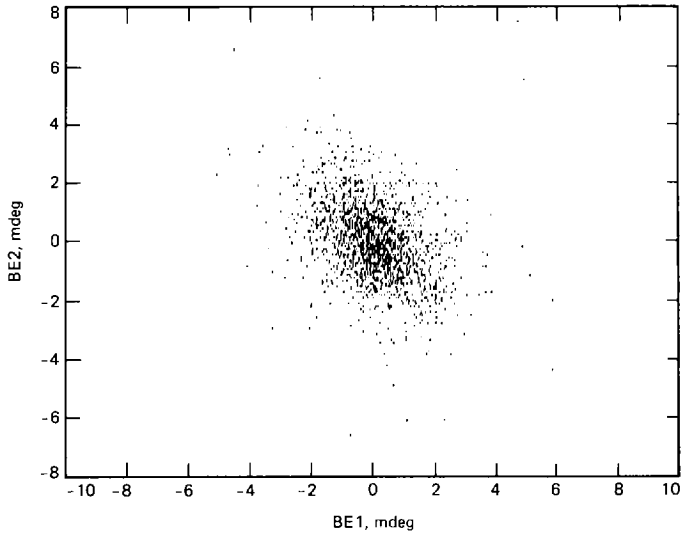

Fig. A-5. Angle offsets calculated from modulation on individual scans: 1,983 scans from Voyagers 1 and 2, DOY 118, 126, 127, 132, 136

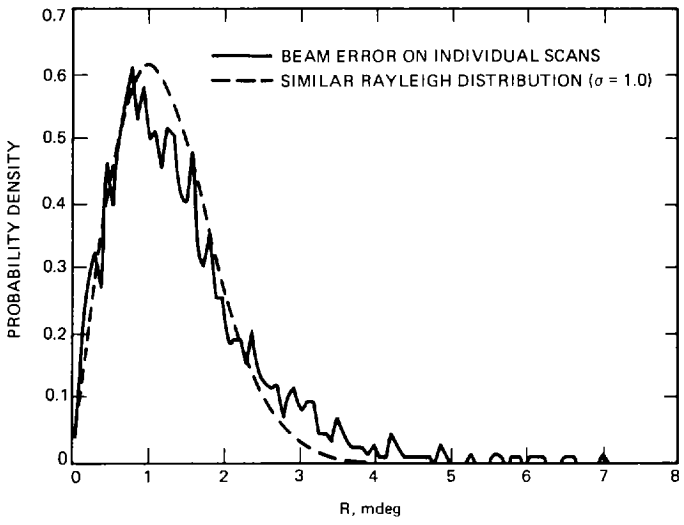

Fig. A-6. Probability density

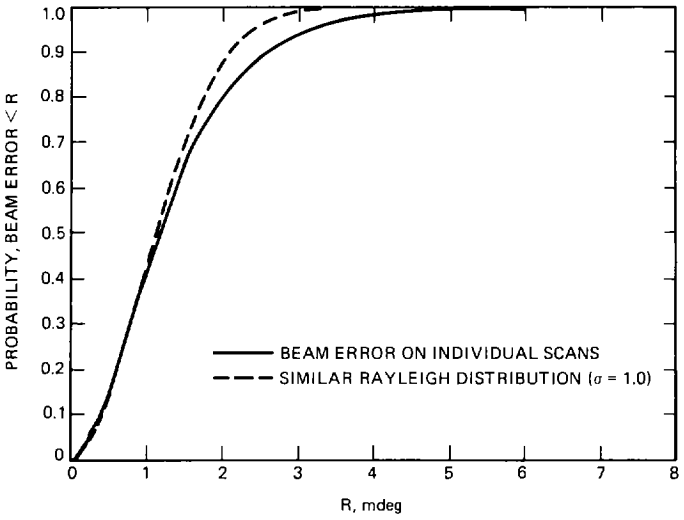

Fig. A-7. Cumulative distribution

Appendix B

Atmospheric Refraction Effects on Elevation Pointing

I. Introduction

Atmospheric refraction causes significant bending of radio waves, especially at low elevation angles. We review the antenna elevation pointing errors resulting from the bending and the methods used to reduce the magnitude of the errors. We also review the importance of the refraction caused errors in performing standard DSN antenna pointing functions.

Methods for calculating the radio wave bending depend on the constituents and their distribution in the atmosphere. Surface pressure, temperature, and relative humidity are useful in characterizing the atmosphere for such calculations.

Presently, the DSN uses a default set of surface atmospheric parameters in the algorithm for calculating refraction correction vs. elevation angle. The parameters define an average surface atmosphere at a particular DSN complex. Use of actual surface atmospheric parameters measured during the epoch of a pass will improve the accuracy of the calculations.

We made measurements of the SPC 10 surface atmosphere at frequent intervals during many of the conscan calibration tracks. The measurements were used as a basis for calculating current refraction corrections that could be compared with the fixed parameter set calculations. The measurements and the results are presented.

The discussion of the results shows that more work on this subject is needed by the DSN, particularly in regard to application of the 70- and 34-m antennas at Ka band. Specific topics for inquiry are cited.

II. Refraction Correction and Its Importance in DSN Applications

A. The DSN Refraction Model

The refraction correction algorithm used in the DSN is the Berman/Rockwell (B/R) model as defined in [B-1] and [B-2]. For the SPC 10 average (default) parameters

Pressure = 901.09 mbars
Temperature = 22.07°C
Relative humidity = 31.57 percent

the refraction correction vs. elevation is as depicted in Table B-1. Also, Table B-1 shows error estimates derived from results by other investigators [B-3], [B-4] and applied to the B/R model.

We will discuss the B/R model and compare it with other models in Section IIC.

The values in column (1) of Table B-1 are true elevation angles. The calculated B/R model values in column (2) show that the refraction correction is large even to mid-range elevations. Column (3) displays the calculated errors in the correction if an average refraction condition for a locale is assumed—it should be representative of our use of default atmospheric parameters. Column (4) displays calculated errors if concurrent surface atmospheric observations are used in the refraction calculations—it should be representative of our results obtained in that way. We show the 2-σ error estimates because they are relevant to conventional communication link reliability considerations, i.e., about 95 percent of the time, the errors would be equal to or less than those shown.

B. The Importance of Refraction Caused Pointing Errors in DSN Applications

Table B-2 shows characteristics of DSN antenna beams. The logic of the table is: Pointing within 0.1 half-power beamwidth (HPBW) in both beam axes, elevation and cross-elevation, produces no more than 0.25 dB degradation or uncertainty in received or transmitted signal level—very satisfactory for all but the most demanding DSN support. Pointing within 0.5 HPBW in elevation produces no more than 3 dB degradation—very satisfactory for all normal signal acquisition operations.

Based on the error estimates of Table B-1 and the antenna beam characteristics of Table B-2, we make the following general observations:

(1) For all normal S-band functions and for normal X-band acquisition, correction for concurrent surface atmospheric conditions *is not necessary*. A suitable average of site conditions should suffice for the refraction calculation—refer to Table B-1, column 3, at elevations >10 degrees.

(2) For precision pointing at X-band, and for all Ka-band functions, correction for concurrent surface atmospheric conditions *is necessary*. The fractional beamwidths for these functions are set boldface in Table

B-2 for emphasis. For Ka-band precision pointing at low elevations, the quality of the correction appears marginal—refer to Table B-1, column 4.

(3) For antenna pointing calibrations, the accuracy objective is <1 mdeg, and correction for concurrent surface atmospheric conditions *is necessary*.

Regarding observation 2, recall that when an antenna is properly functioning in the conscan mode, all pointing errors that are slowly varying compared to the scan period, including refraction effects, are removed.

C. Discussion of the Berman/Rockwell and Other Radio Frequency Refraction Models

1. The Berman/Rockwell model. The basic approach in the B/R radio refraction model derivation (cf. [B-1], [B-2]) is to empirically match a pedigreed tabulation for optical refraction with an analytic function. The simplified form of the function (Ropt) applicable for elevation angles >5 degrees is:

$$\text{Ropt} = [\text{Fp(surf. press.)}] \times [\text{Ft(surf. temp.)}] \times [\text{Fe(el. angle)}] \quad \text{(B-1)}$$

Then, the radio refraction model (Rrf) is obtained by multiplying the optical refraction of Eq. (B-1) by a "wet" term that includes the effects of water vapor in the atmosphere:

$$\text{Rrf} = \text{Ropt} \times [\text{Fw(surf. press., temp., rel. humidity)}] \quad \text{(B-2)}$$

Equation (B-2) provides a good approximation of the complete B/R algorithm—within approximately 2 mdeg at 5 degrees elevation, 0.6 mdeg at 10 degrees elevation. For the SPC 10 default values for surface pressure, temperature, and relative humidity, Eq. (B-2) is

$$\text{Rrf(def)} = \text{Fp(901.09 mbar)} \times \text{Ft(22.07°C)} \times \text{Fe(el. angle)} \times \text{Fw(901.09 mbar, 22.07°C, 31.57 percent)}$$

Radio refraction values based on current surface observations, Rrf(obs), can be calculated similarly. Note that in the simplified B/R model, all elevation dependence is contained in the function Fe, and Fe is independent of atmospheric effects (Eqs. (B-1), (B-2)). Thus, a refraction table based on surface observations can be made directly from the default table:

$$\text{Rrf(obs)} = \text{Rrf(def)} \times [\text{Fp} \times \text{Ft} \times \text{Fw(obs)} / \text{Fp} \times \text{Ft} \times \text{Fw(def)}] \quad \text{(B-3)}$$

We have used the convenient relationship Eq. (B-3) to reduce and analyze our experimental data.

To our knowledge, no significant experimental validation of the B/R refraction model and its expected errors has been done. In the next paragraphs we compare the B/R model with other models.

2. Other radio refraction models. Radio refraction studies of Bean and Dutton [B-3] and Crane [B-4] use an approach different from that of Berman/Rockwell. Their basic technique is:

(1) Collect a large data set of atmospheric parameters vs. height above the surface using radiosondes. Include concurrent surface observations.

(2) Calculate the trajectory of the radio ray through each of the atmospheric profiles provided from the radiosonde observations. Each calculation provides an estimate of elevation refraction of a radio signal from above the atmosphere. Also, from the set of calculations, some statistics of the elevation refraction are provided.

(3) From all the calculations, plot for individual elevation angles the elevation refraction (Rrf) vs. the N number of the surface refractive index (Ns), derived from the concurrent surface observations. Then, observe that Rrf vs. Ns for each elevation angle has the form:

$$\text{Rrf} = a + b \times \text{Ns} \quad \text{(B-4)}$$

(4) For each elevation angle, do a straight line least squares best fit of the Rrf vs. Ns data and determine the regression coefficients, a and b, in Eq. (B-4). Calculate the statistics of the data fit to the lines.

Using the above techniques, the individually calculated results of Bean and Dutton, and Crane, are quite consistent. Bean and Dutton show some experimental results that support their calculations.

Finally, in their theoretical development, Bean and Dutton arrive at a very simple approximation for radio refraction:

$$\text{Rrf} = \text{Ns} \times \cot(\text{el.}) \times 57.3 \times 10 \wedge -6 \text{ (mdeg)} \quad \text{(B-5)}$$

Equation (B-5) is useful above 10 degrees elevation.

3. Comparison of B/R and the other models. We have calculated refraction tables for the SPC 10 default atmospheric parameters using Eq. (B-4) and the regression coefficients from

Bean and Dutton ([B-3], Table 9.9), and from Crane ([B-4], Table II). Also, we calculated Eq. (B-5).

Figure B-1 compares the complete B/R algorithm with the other refraction models as a function of elevation angle (B/R minus the others). The agreement between the B/R, Bean and Dutton, and Crane models is quite good (<2 mdeg) over the range of elevations presented. It lends confidence to our use of the B/R model. The range of usefulness of the simple Eq. (B-5) is displayed.

The statistics cited in paragraphs 2(2) and 2(4) above were taken from Crane ([B-4], Fig. 3 and Table II) to develop the estimated errors in our Table B-1, columns (3) and (4).

III. SPC 10 Surface Atmosphere Observations

A. Introduction

We collected surface atmospheric data at regular intervals during most of the Voyager passes that we observed. The data were used to upgrade the refraction correction provided by the standard default values. The objectives were to provide improved correction of refraction errors during the Saturn radar support, and to provide better data for development of the antenna error model. Also, we wanted to develop and demonstrate refraction correction techniques for future use in the operational DSN.

The methods of collecting and processing the data are described. Summary analyses of the data from DOY 120 to 142 are presented and discussed.

B. Data Collection and Processing

All atmospheric data were hand collected by station personnel, typically at 1 hour intervals. Barometric pressure was read from the MMA display; wet and dry bulb temperatures were read from a Bendix Friez Psychron, model 566 series psychrometer.

Three PC programs were developed to process and apply the atmospheric data: REFCORR, HUM-PSY, and CONCORR. REFCORR was used for on-site refraction correction, and HUM-PSY and CONCORR were used for off-site antenna model development. The functions of the programs are shown in the block diagram, Fig. 3 of this article's main text.

REFCORR computes the elevation offset error resulting from the use of default rather than current atmospheric weather parameters. It requires inputs of wet and dry bulb temperatures, atmospheric pressure, and elevation angle at the time of the readings.

From the surface atmospheric observations, REFCORR computes the relative humidity. Then, using the complete B/R algorithm, it computes the refraction correction for the observed surface atmosphere. Also, it computes the correction for the default surface atmosphere. The two corrections are differenced, giving an estimate of the error in elevation at the time of the observations.

The results are printed and displayed on the screen. A preliminary procedure, "Antenna Pointing Refraction," dated 19 May 1987, describing the operation of REFCORR and the psychrometer, was prepared and issued by M. Wert.

HUM-PSY makes a file of temperature, pressure, and relative humidity values, time-tagged at 15 minute intervals. It requires inputs of wet and dry bulb temperatures, atmospheric pressure, and time of the readings. Relative humidity is calculated as in REFCORR. The values at the reading times are linearly interpolated to create the 15 minute values. HUM-PSY provides inputs to CONCORR.

CONCORR is used to provide refraction correction of conscan files for development of improved antenna pointing error models.

Surface atmospheric data applicable to a conscan data point is determined by selecting data points from the HUM-PSY file adjacent to the time of the conscan point, and then linearly interpolating between them. CONCORR then calculates the refraction correction using the interpolated surface weather data in the complete B/R algorithm. It also calculates the default refraction correction.

The refraction correction from the surface observations is subtracted from the default correction. The result is added to the conscan elevation offset, providing a corrected elevation offset. CONCORR stores the data in a file formatted for use in the antenna error model linear least squares fitting program, PHO9; it also provides plots of corrected elevation offsets vs. time using the companion plotting program, REFPLOT (cf. Fig. B-2).

C. Analysis of SPC 10 Surface Atmosphere Data

We have analyzed the surface atmosphere data taken from DOY 120 to DOY 142. During that time, consistent surface atmosphere observations were made concurrently with several good Voyager spacecraft conscan tracks and one Saturn blackbody track. The atmosphere data are discussed here; results of use of those data in correcting elevation pointing errors are discussed in the next section.

As discussed in Section IIC, a good approximation of the B/R refraction for current surface observations is obtained as the product of the default refraction and the ratio of the surface atmosphere dependent parameters, Fp, Ft, and Fw [from Eq. (B-3)]:

$$Rrf(obs)/Rrf(def) = Fp \times Ft \times Fw(obs)/Fp \times Ft \times Fw(def)$$

Figure B-2 shows plots of calculated Rrf(obs)/Rrf(def) ratios for the surface observations during the period. For example: on DOY 120, the ratio varied between 1.045 and 1.08; at 10 degrees elevation, the default refraction correction is 85.0 mdeg; the calculated correction from the surface observations varied between 85 X 1.045 = 88.8 mdeg and 85 X 1.08 = 91.8 mdeg.

It is evident that the Fig. B-2 ratios are fairly well behaved and slowly varying during any single pass period. However, for passes separated by several days, the ratios vary widely. One measurement each day is about five times better than none.

A representative measure of the sensitivity of the refraction ratios to the surface atmospheric parameters—pressure, temperature, and relative humidity—is available from our measurements. The ranges observed of the parameters are:

Pressure: 895–905 mbar
Temperature: 7–27.5°C
Relative Humidity: 15–81 percent

Setting two of the parameters to default values, and varying the third over the ranges indicated, show that the angular refraction change caused by the relative humidity variations was about 5 times that from the temperature variations and 30 times that from the pressure variations. If humidity changes are forecast, expect significant changes in radio refraction.

Figure B-3 shows daily averages of the Rrf(obs)/Rrf(def) ratios. The significant changes over several days are clearly illustrated.

From the data in Fig. B-3, we can calculate the variance of the elevation error resulting from use of the default rather than the observed atmospheric parameters. For example, at 10 degrees elevation, the calculated mean (+3.3 mdeg) plus 2-σ error (2 X 5.10 mdeg) is 13.5 mdeg, to be compared to 11.6 mdeg given in column (3) of Table B-1—values at other elevations have the same relative comparison. The comparison should be considered qualitative, because our data sample is tiny—the 90 percent confidence interval on sigma is 3.8 to 8.0 mdeg.

IV. Elevation Offsets Using Surface Atmospheric Measurements

A. Introduction

We have analyzed elevation offset data from the Voyager conscan and Saturn beam scan passes of DOY 120 to DOY 142. Elevation offsets obtained using the default refraction correction are compared with calculated offsets using concurrent surface atmospheric observations.

The results show that the surface observations are useful, but leave some unanswered questions.

B. Elevation Offsets From Individual Passes

Observed offsets based on default correction, and calculated offsets based on surface observations, are plotted in Figs. B-4 through B-11. Three different antenna systematic error tables (SETBLs) were used during the period, but the plotted offsets have all been adjusted to a common SETBL, 4X31C. The calculated offsets are from the simplified B/R algorithm.

The figures show that, except for DOY 127, the calculated offsets are of smaller magnitude (closer to zero elevation error) than the default offsets. Unfortunately, we don't really know what the true elevation error should be, because of possible errors in the antenna pointing system. Examination of the average offsets can provide some insight into the matter.

C. Elevation Offset Averages

Figure B-12 shows the pass averages of the default and calculated offsets. Globally, the calculated offsets are an improvement. However, they are certainly not negligible, especially after DOY 125. After DOY 125 there is an apparent bias in the calculated offsets of about +3 mdeg—about that bias they behave fairly well.

The signatures of all offset curves, default and calculated, show increases at low elevation angles (cf. Figs. B-4 through B-11). Figure B-13 shows the average of all default and calculated offsets vs. elevation angle. The residual calculated offsets are large at 10 degrees and significant at 15 degrees. They are about three times the 2-σ errors expected using concurrent surface atmospheric observations (compare column (4) of Table B-1).

The source of the apparent large errors, especially at low elevation angles, is not understood:

(1) The B/R refraction algorithm was shown to agree fairly well with other models down to 5 degrees elevation—can they all be in equal error?

(2) Are we doing something wrong in processing or applying the surface observations?

(3) Is there some unidentified error characteristic of the antenna system that has such a steep angular gradient?

V. Summary Observations on Refraction Effects

(1) Refraction causes large errors in elevation angle. Correction based on average site (default) atmospheric parameters is adequate for all S-band and for normal X-band acquisition operations. Antenna calibrations, precision X-band, and all Ka-band operations require correction based on concurrent surface atmospheric observations.

(2) Results from the DSN's Berman/Rockwell algorithm for calculating refraction from surface atmospheric parameters agree fairly well with other formulations.

(3) Large changes in refraction tend to occur over several days, while changes within the length of a pass tend to be very much smaller.

(4) The results in improving refraction correction by using concurrent surface atmospheric observations were significantly less accurate than expected. At low elevations, the errors are unaccountably large—although that may not be a refraction effect.

(5) Further work has been identified to refine and demonstrate the model of the effects of atmospheric refraction on antenna pointing:

(a) Use more recent literature on radio refraction models and the experimental results establishing their accuracy (the latest reference used here was from 1976).

(b) Find and remove the cause of the large low elevation errors.

(c) Establish a field experimental program to demonstrate refraction corrections of the required accuracy to support antenna pointing calibrations at X-band (8.5 GHz) and future Ka-band (34 GHz), in preparation for a network operational capability.

References

[B-1] A. L. Berman and S. T. Rockwell, *New Optical and Radio Frequency Angular Tropospheric Refraction Models for Deep Space Applications*, Technical Report 32-1601, Jet Propulsion Laboratory, Pasadena, California, November 1, 1975.

[B-2] A. L. Berman, "Modification of the DSN Radio Frequency Angular Tropospheric Refraction Model," *DSN Progress Report 42-38*, vol. January–February 1977, Jet Propulsion Laboratory, Pasadena, California, pp. 184–186, April 15, 1977.

[B-3] B. R. Bean and E. J. Dutton, *Radio Meteorology*, New York: Dover Publications, Inc., especially Chapters 1 and 8, 1968.

[B-4] R. K. Crane, "Refraction Effects in the Neutral Atmosphere," *Methods of Experimental Physics*, New York: Academic Press, Chapter 2.5, 1976.

Table B-1. SPC 10 refraction correction and errors vs. elevation angle

(1) Elevation angle (deg)	(2) Refraction correction[a] (mdeg)	(3) Estimated 2-σ error[b] with average atmospheres (mdeg)	(4) Estimated 2-σ error[b] with surface observations (mdeg)
5.0	156.9	21.3	3.3
10.0	85.0	11.6	1.8
15.0	58.1	7.9	1.2
20.0	43.7	5.9	0.9
30.0	27.2	3.7	0.6
40.0	18.5	2.5	0.4
60.0	9.0	1.2	0.2
90.0	0.0	0.0	0.0

[a] B/R model using SPC 10 default parameters.
[b] From interpretation of data by Crane [B-4].

Table B-2. Approximate 0.1 and 0.5 half-power beamwidths (HPBWs) of DSN antennas

Frequency band	70-m 0.1 HPBW/0.5 HPBW (mdeg)	34-m 0.1 HPBW/0.5 HPBW (mdeg)
S	11/57	23/114
X	**3**/15	**6**/30
Ka	**0.8/4**	**1.6/8**

The fractional beamwidths for these functions are set boldface for emphasis.

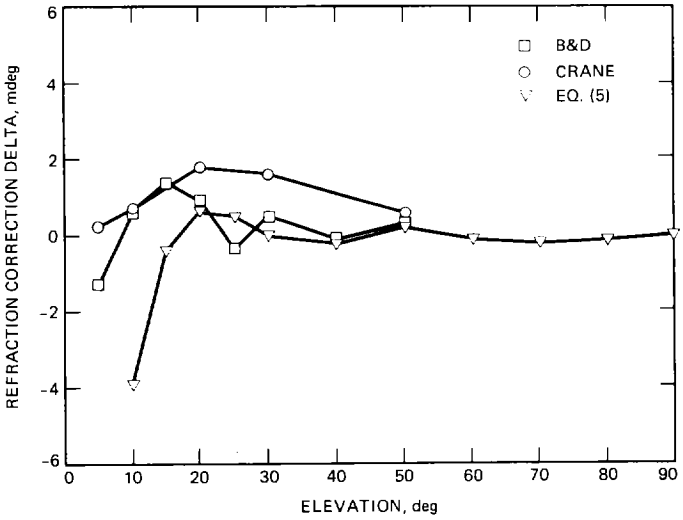

Fig. B-1. Deltas (B/R—other models); GDSCC default parameters

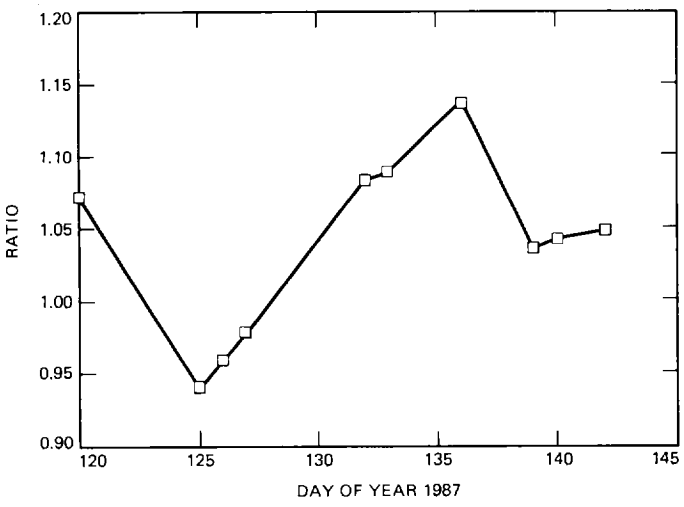

Fig. B-3. Daily average observed/default refraction ratios

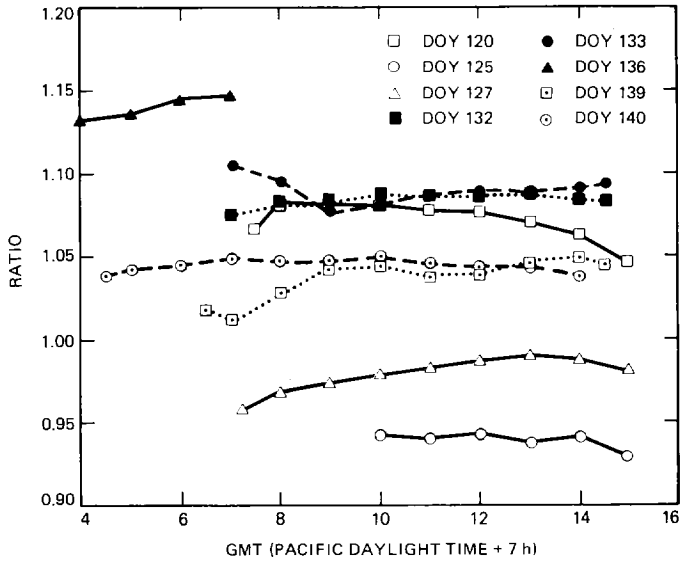

Fig. B-2. Hourly observed/default refraction ratios

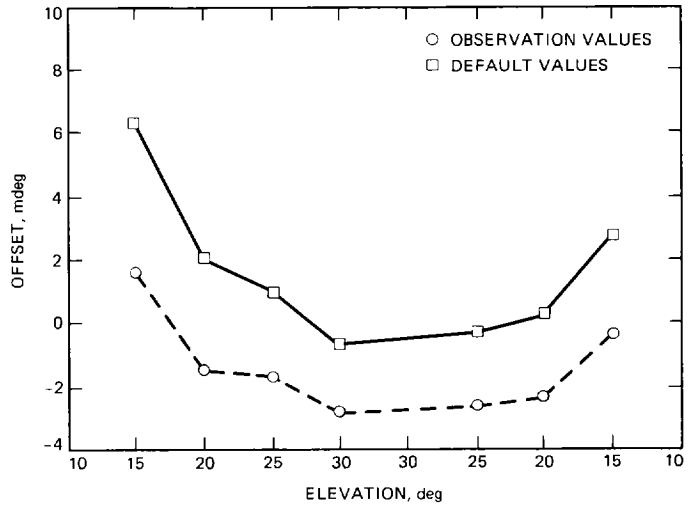

Fig. B-4. Elevation offsets: Voyager 2 DOY 120 (corrected to SETBL 4X31C)

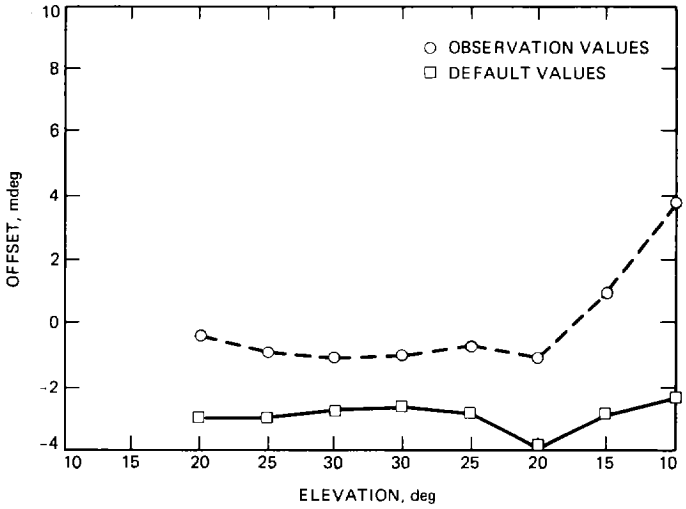

Fig. B-5. Elevation offsets: Voyager 2 DOY 125 (corrected to SETBL 4X31C)

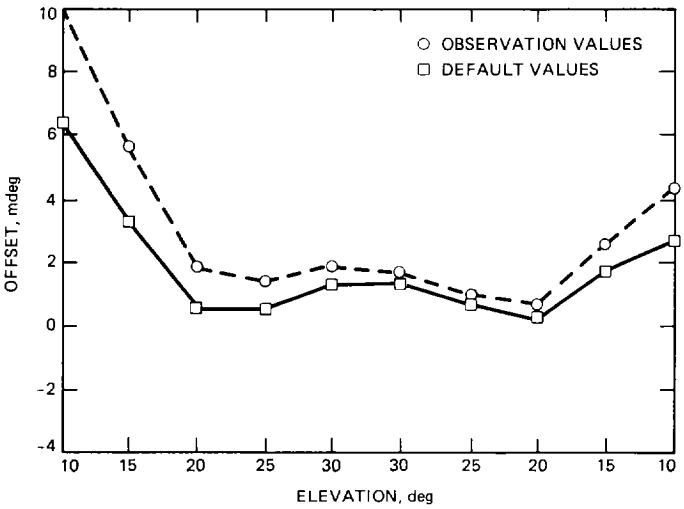

Fig. B-6. Elevation offsets: Voyager 2 DOY 127 (corrected to SETBL 4X31C)

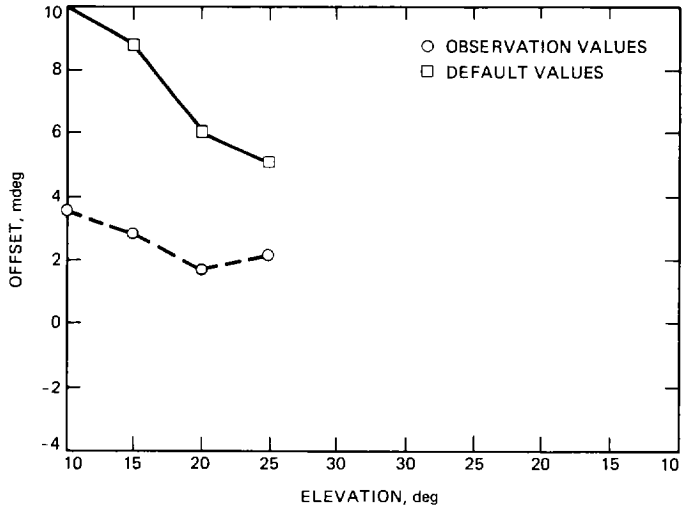

Fig. B-7. Elevation offsets: Voyager 2 DOY 133 (corrected to SETBL 4X31C)

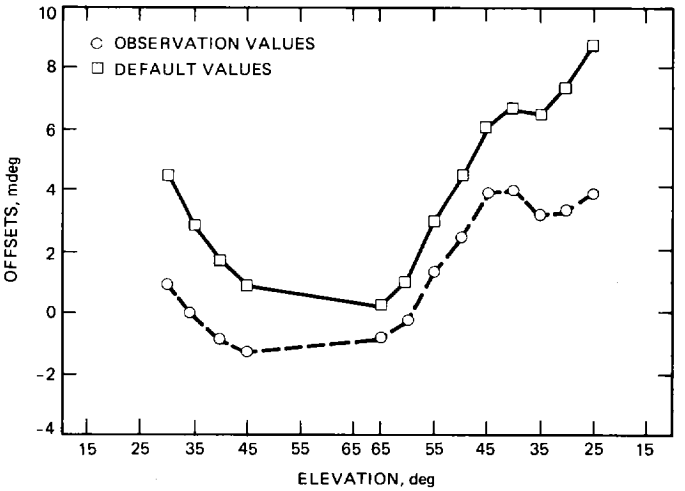

Fig. B-8. Elevation offsets: Voyager 1 DOY 136 (corrected to SETBL 4X31C)

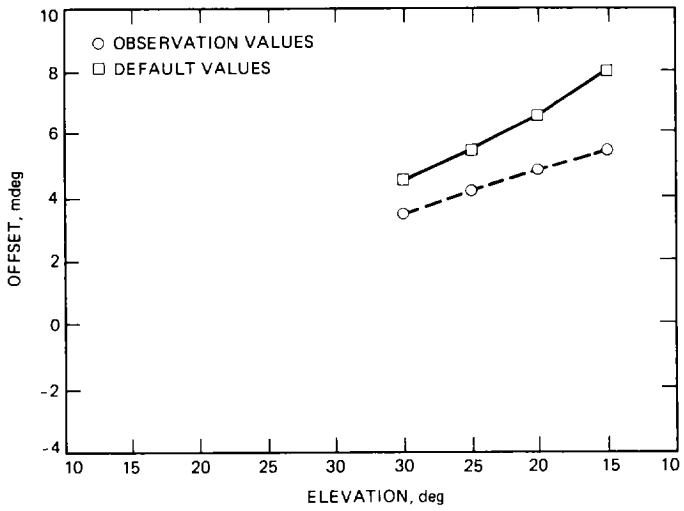

Fig. B-9. Elevation offsets: Saturn blackbody scans DOY 139 (SETBL 4X31C)

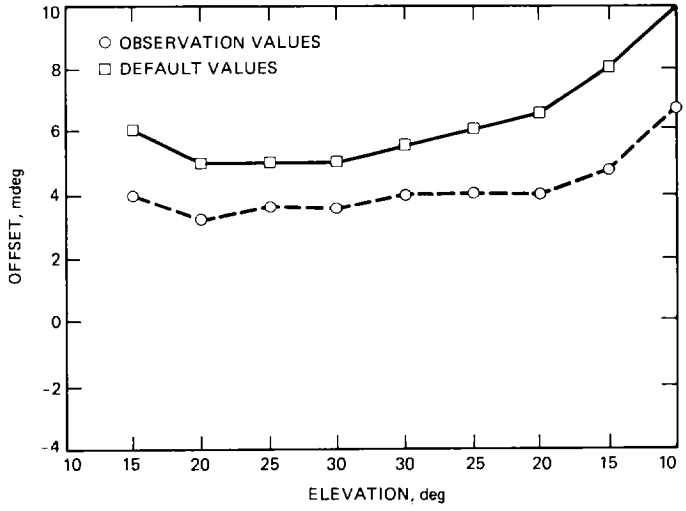

Fig. B-11. Elevation offsets: Voyager 2 DOY 142 (SETBL 4X31C)

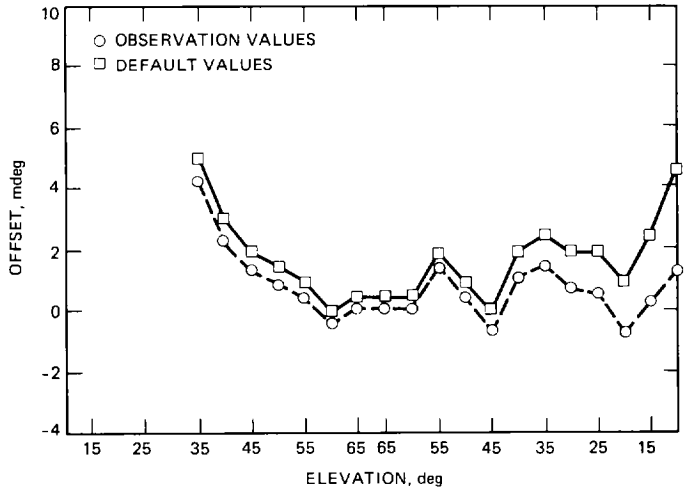

Fig. B-10. Elevation offsets: Voyager 1 DOY 140 (SETBL 4X31C)

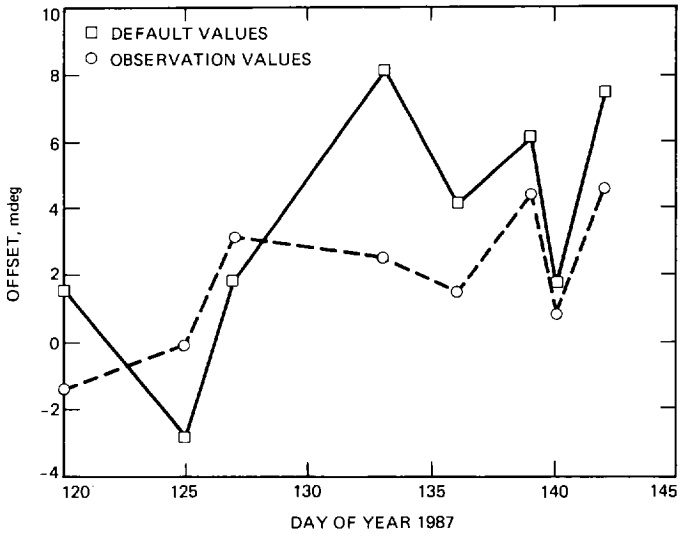

Fig. B-12. Average default and corrected elevation offsets (corrected for surface observations and to SETBL 4X31C)

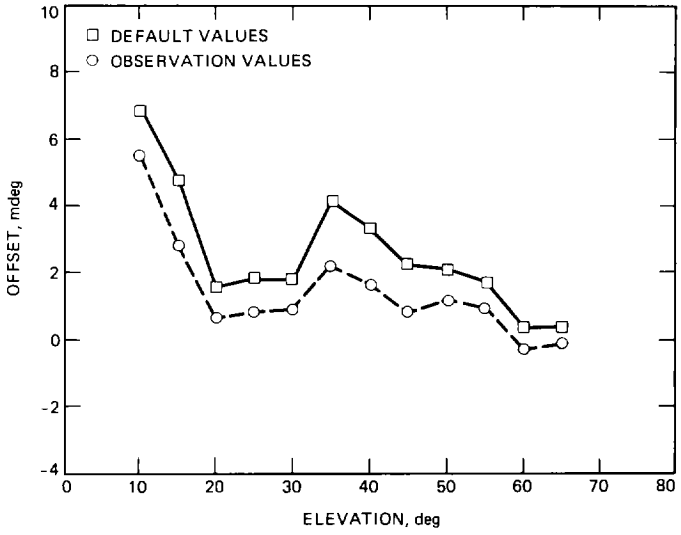

Fig. B-13. Average elevation offsets (corrected to SETBL 4X31C)